national accelerator laboratory

FERMILAB-Pub-74/105-EXP
7200.037

(Submitted to Physical Review)

pp INTERACTIONS AT 300 GeV/c: γ AND NEUTRAL STRANGE PARTICLE PRODUCTION

A. Sheng, V. Davidson, A. Firestone, F. Nagy, and C. Peck
California Institute of Technology, Pasadena, California 91109

and

F. T. Dao, R. Hanft, J. Lach, E. Malamud, and F. Nezrick
Fermi National Accelerator Laboratory, Batavia, Illinois 60510

and

A. Dzierba
Indiana University, Bloomington, Indiana 47401

and

R. Poster
University of California, Los Angeles, California 90024

December 1974

FERMILAB-Pub-74/105-EXP
CALT-68-480
IND-COO-2009-89
UCLA-1102

pp Interactions at 300 GeV/c: γ and Neutral Strange Particle Production*

by

A. Sheng, V. Davidson, A. Firestone, F. Nagy, and C. Peck

California Institute of Technology, Pasadena, California, 91109

F. T. Dao†, R. Hanft, J. Lach, E. Malamud, and F. Nezrick

Fermi National Accelerator Laboratory, Batavia, Illinois, 60510

A. Dzierba

Indiana University, Bloomington, Indiana, 47401

R. Poster

University of California, Los Angeles, California, 90024**

ABSTRACT

In a 35000 picture exposure of the Fermilab 30-inch hydrogen bubble chamber to a 300 GeV/c proton beam 1863 neutral V^o's were measured. The inclusive cross sections for γ, K^o_s, Λ^o/Σ^o and $\bar{\Lambda}^o/\bar{\Sigma}^o$ are 257 ± 18 mb, 7.3 ± 0.6 mb, 3.6 ± 0.4 mb and 1.0 ± 0.3 mb respectively. The correlation with charged particles and other inclusive features are studied.

* Work supported in part by the U. S. Atomic Energy Commission.
**Work supported in part by the National Science Foundation (GP33565).
† Present address: Physics Department, Tufts University, Medford, Mass. 02155.

I. Introduction.

One of the most interesting results that has emerged from the Fermilab bubble chamber experiments[1,2,3] concerns the production of π^o's and neutral strange particles. In particular, these experiments have shown through studies of the γ-conversions in the chamber that there is a strong correlation between the production of neutral and charged pions. While those data suggest a similar behavior between K_s^o's and charged particles the effect is not as striking due to the limited statistics available so far. The Λ^o also shows an interesting feature in that it is predominantly produced in the fragmentation region, with a very low central "plateau". On the other hand, the $\bar{\Lambda}^o$ appears to be produced exclusively in the central region. However the very limited statistics on $\bar{\Lambda}^o$ leaves the question open as to whether the central region is dominated by $\Lambda^o - \bar{\Lambda}^o$ production. In this paper we report on these and other inclusive features of the V's. Here V is used to refer to both the strange neutrals as well as the γ-conversions pairs. The data represent a six-fold increase in the number of events over what was previously reported at this energy[3]. It is important to note that the 303 GeV/c data reported in reference 3 are not included in this paper and the results should be regarded as from two separate experiments.

II. Data.

The data of this experiment were from a 35000 picture exposure of the Fermilab 30-inch hydrogen bubble chamber to a 300 GeV/c proton beam. Two independent scans were performed over the entire film sample, and 1924 events were found to have one or more apparent V's that appeared to be associated with the primary interactions. This corresponded to 2277 V's. The rules followed in the scans have been described in a previous publication[4]. The efficiency

of each scan was found to be 85% for V detection, which implied that the combined efficiency of both scans was greater than 97%. An unbiased sample of 1863 V's were measured at the Film Analysis Facilities of the Fermilab. During the course of the measurements 89 additional V's were found and measured. This increased the total efficiency to close to 100%. Out of the above sample 65 were found not to be V's under close inspection, and 28 were impossible to measure. The measurements were processed using the standard TVGP and SQUAW programs.

All the V's that failed to reconstruct satisfactorily were remeasured. After two measurements 840 V's still had unsatisfactory TVGP results and were measured a third time using the high magnification tables at the Fermilab. There were 1252 V's within the fiducial volume[5], of which 1231 V's passed TVGP after the three measurements, and were used in kinematic fits. Of these V's 94 were not consistent with any 2-constraint hypothesis, and therefore were considered as not associated with the primary interaction; 10 had successful 2-constraint fits but failed to give a satisfactory 3-constraint fit[6].

About 1/4 of the V's produced more than one 3-constraint fit. In about half of these cases the kinematic ambiguity could be resolved using ionization. The unresolvable V's were classified according to the transverse momentum in the laboratory between the V and its negative track[7]. This was effective in distinguishing the γ's, and those K_s^o's that decay with a helicity angle $> \sim 30^o$ in their rest frame. The $K_s^o - \Lambda^o(\bar{\Lambda}^o)$ ambiguities that remained (less than 15% of the ambiguous V's) were all classified by choosing the hypothesis giving the smallest value for the quantity $|m_{2c} - m_o|/\sigma_{2c}$, where m_{2c} and σ_{2c} are the 2 constraint fitted mass and its error[6], and m_o is the true mass of the V in that fit hypothesis.

In order to calculate the decay or conversion probabilities fiducial cuts on both the primary and V vertices were imposed[5]. The fiducial volumes were chosen such that there were at least 8 cm of potential decay path length and 6 cm of measurable charged tracks. An additional cut on the minimum distance of the V from the primary vertex was also used in order to account for close-in V's which were misidentified as primary tracks[8]. A detection probability was then calculated for each V based on this minimum distance cut-off and the potential path length inside the chosen fiducial volume.

The inclusive cross sections were calculated by using only the V's going backward in the center of mass. This was because the statistics of the strange neutrals in the forward hemisphere was extremely poor due to the low decay probabilities in that region. There was also a depletion of the forward going γ's with longitudinal rapidity in the center of mass $y > 1.5$. This depletion is mostly due to the confusion caused by the charge tracks in the very forward direction in the bubble chamber. Fig. 1 shows $\frac{d\sigma}{dy}$ for the γ's. There is a forward-backward asymmetry as indicated by the ratio $R = (F - B)/(F + B) = -0.073 \pm .046$ where F(B) is the number of forward (backward) going γ's after correcting for the detection probability. However this asymmetry is entirely due to γ's with $|y| > 1.5$ where $R = -.225 \pm .072$, as compared to $R = -.006 \pm .058$ for $|y| < 1.5$. A further correction was made for the γ's since the pair-production cross section[9] drops quickly for photon momenta below 100 MeV/c in the laboratory. These γ's were removed and instead we used the γ's symmetric in the Peyrou plot to these low energy γ's. The cross sections were then calculated by doubling the number of V's in the backward hemisphere and weighing each V by the inverse of its detection probability and, in the case of the strange neutrals, the inverse of the branching ratio into charged particles. The average detection probabilities for the backward going V's were $P_{\gamma} = 0.016$, $P_{K^0_s} = 0.59$,

$P_{\Lambda^o} = 0.60$, and $P_{\bar{\Lambda}^o} = 0.33$. The large difference in P_{Λ^o} and $P_{\bar{\Lambda}^o}$ reflects the different kinematic regions where the Λ^o and $\bar{\Lambda}^o$ were produced. The normalization was obtained by scaling the measured sample to the sample used in determining the total cross section in reference 4 after correcting for all processing losses.

III. Cross Sections.

The calculated cross sections are $\sigma_\gamma = 257 \pm 18$ mb, $\sigma_{K_s^o} = 7.3 \pm 0.6$ mb, $\sigma_{\Lambda^o/\Sigma^o} = 3.6 \pm 0.4$ mb and $\sigma_{\bar{\Lambda}^o/\bar{\Sigma}^o} = 1.0 \pm 0.3$ mb. The corresponding average numbers produced per inelastic interaction are $\langle n_\gamma \rangle = 7.84 \pm 0.55$, $\langle n_{K_s^o} \rangle = 0.22 \pm 0.02$, $\langle n_{\Lambda^o} \rangle = 0.11 \pm 0.01$ and $\langle n_{\bar{\Lambda}^o} \rangle = 0.03 \pm 0.01$. Tables 1, 2 and 3 show the topological cross sections as well as the number of weighted and unweighted γ's, K_s^o's and Λ^o's.

The inclusive topological cross sections for the π^o, K_s^o and Λ^o can be plotted according to the semi-inclusive KNO scaling equation[10,11].

$$\frac{\langle n \rangle}{\langle n_I \rangle} \frac{\sigma_I(n)}{\sigma_{inel}} = \Phi\left(\frac{n}{\langle n \rangle}\right)$$

where $\langle n \rangle$ and $\langle n_I \rangle$ are the average numbers per inelastic collision for charged particles and the inclusive particle studied, $\sigma_I(n)$ is the inclusive cross section associated with n charged particles and σ_{inel} is the total inelastic cross section. The data in Fig. 2 show that within the level of statistics all three particles follow the same shape, and are quite consistent with the form for $\Phi\left(\frac{n}{\langle n \rangle}\right)$ obtained in reference 10 using inclusive π^o data from pp and $\bar{p}p$ experiments.

There are 10 V's that gave successful 2 constraint fits but failed to fit any 3 constraint hypothesis. Therefore these V's are associated with the primary interaction but are inconsistent with being either γ's, K_s^o's, Λ^o's or

$\bar{\Lambda}^{o}$'s. In order to determine an estimate of the cross section for possible new neutral particles that decay into two charged particles we examined the transverse momentum p_T^V in the laboratory between the V and one of its tracks. Only one out of the 10 candidates have p_T^V greater than what is allowed by the kinematic limits of the known particles. These V's have been remeasured at least once and the results are stable under remeasurements. Therefore we conclude that there are 10^{+3}_{-9} V's that are possibly new particles. This corresponds to a cross section of 75^{+23}_{-68} μb for the production of possible new neutral particles without correcting for detection probability due to decay lifetime.

IV. Inclusive γ Production.

If we assume that all γ's come from the decay of π^o's the inclusive π^o cross section is 129 ± 9 mb. This is in agreement with the value of $(\sigma_{\pi^+} + \sigma_{\pi^-})/2 = 116 \pm 3$ mb calculated from reference 4 under the assumptions that on the average there is one proton produced per inelastic collision and all other produced charged particles are pions and kaons with $\sigma_{K^+} + \sigma_{K^-} = \sigma_{K^o} + \sigma_{\bar{K}^o} = 14.6 \pm 1.2$ mb. In the subsequent analysis data from both center of mass hemispheres are used for the γ's, with an additional weight of 1.68 assigned to those γ's with $y > 1.5$ to account for the forward-backward asymmetry. In order to investigate the correlation between the neutral and charged pions we have calculated the average number of π^o's produced per inelastic interaction, $< n_o >$, as a function of negative charge multiplicity n_-. Fig 3a shows $< n_o >$ versus n_-. As was shown earlier[10], a monotonic increase in $< n_o >$ with n_- is evident. The straight line represents a fit to the form

$$< n_o > = \alpha\, n_- + \beta$$

over the range where $n_- \leq 9$, with $\alpha = 0.50 \pm 0.10$, $\beta = 2.26 \pm 0.32$ and a χ^2 of 5.25 for 8 degrees of freedom.

Many models have been proposed to explain this correlation between the neutral and charged pions, usually using the idea of cluster formation[12]. Recently evidence has been presented that such a correlation may be caused by the presence of two separate components in the production process. It was shown that in $\bar{p}p$ interactions at 19 GeV/c, $< n_o >$ has little dependence on n_- when considered separately for annihilation and non-annihilation events[13]. It is speculated that in pp interactions the diffractive and non-diffractive processes may exhibit this same behavior.

In order to examine this hypothesis we separate our data into "diffractive" and "non-diffractive" events for $n_- = 0$, 1, and 2. Events in which the slowest track is consistent with being a proton by ionization, and the square of the missing mass against this "proton" is less than 50 GeV^2, are considered as beam diffraction events. We find for these events $< n_o >_{diff} = 1.4 \pm 0.9$, 2.2 ± 1.1 and 3.7 ± 3.7 for $n_- = 0$, 1, and 2 respectively. In order to calculate $< n_o >_{non}$, we assume that the cross section for target diffraction equals that for beam diffraction, and that for $n_- > 2$ the diffraction cross section is neglible. Fig. 3b shows $< n_o >_{non}$ as a function of n_-. Although a fit to a constant gives $< n_o > = 4.3 \pm 0.3$ with a χ^2 of 9.3 for the 10 data points, nevertheless there is some indication of a systematic deviation from $< n_o >_{non} = 4.3 \pm 0.3$, which would not seem to support the two component hypothesis. The open circles in Fig. 3b indicate the upper limits for $< n_o >_{non}$ at $n_- = 1$ and 2, which we estimate by taking $\sigma_{diff} = 2.0 \pm 0.2$ mb and 0.6 ± 0.2 mb respectively[14]; and also assume that no π^o's are produced in diffractive events. The same systematic deviation from a constant $< n_o >_{non}$ still persists.

The value for the correlation parameter $f_2^{o-} = < n_- n_o > - < n_o > < n_- >$ is 2.0 ± 0.6 where $n_-(n_o)$ is the number of negative particles (π^o's) in an inelastic event. This agrees well with previous results[10], and using the data from reference 4 for $f_2^{+-} = 3.24 \pm 0.13$, and with $f_2^{--} = f_2^{+-}/2$ we observe the well known relation $f_2^{+-} > f_2^{o-} > f_2^{--}$.

In Figs. 4a, b, c, and d we show $\frac{1}{\sigma_{inel}}\frac{d\sigma}{dx}$ and $\frac{1}{\sigma_{inel}}\frac{d\sigma}{dp_T^2}$ as well as the integrals over p_T^2 and x of the invariant cross section $\frac{2E}{\pi\sqrt{s}}\frac{d^2\sigma}{dx dp_T^2}$ where E, p_T and x are all calculated in the over-all center of mass for the γ. It is clear when compared with lower energy data that at Fermilab energies scaling has been reached within the level of statistics. The average values of p_T and p_L for the γ are 0.25 ± 0.02 and 0.45 ± 0.04 GeV/c respectively.

V. Inclusive K_s^o Production.

The K_s^o's are produced entirely in the central region as shown by the longitudinal rapidity distribution in Fig. 5. There is no evidence of a plateau in the region $|y| < 1$. However the ∿ 2 mb height near y = 0 is consistent with the short range order (SRO) hypothesis[15] which gives

$$\sigma_{incl} = \sigma_h \ln \frac{s}{s_o}$$

where σ_h is the height of the rapidity plateau, and s_o is a constant. Using σ_h = 2 mb SRO predicts an increase of about 0.8 mb in $\sigma_{K_s^o}$ from 200 GeV to 300 GeV. This agrees well with $\sigma_{K_s^o}$ = 6.5 ± 0.85 mb from reference 2 and our value of 7.4 ± 0.6 mb.

In Fig. 6a we show $< n_{K_s^o} >$ versus n_-. There is good indication for a similar correlation with n_- as the π^o's. The straight line is a linear fit to the form

$$< n_{K_s^o} > = \alpha n_- + \beta$$

for $n_- \leq 7$. Here $\alpha = 0.043 \pm 0.007$ and $\beta = 0.052 \pm 0.015$ with a χ^2 of 23 for 6 degrees of freedom, whereas the best fit to a constant gives a χ^2 in excess of 55.

The differential cross sections in terms of the scaling variables x and p_T^2 are shown in Figs. 7a, b, c, and d. Here again the present data scales within errors when compared with lower energy Fermilab data[1,2]. Recently the authors proposed a new set of scaling variables[16], which appear to apply to inclusive distributions regardless of initial state and energy. The

proposed scaling variables are $p_L / \langle p_L \rangle$ and $p_T / \langle p_T \rangle$. In Figs. 8a and b we have plotted the quantities $\frac{\langle p_L \rangle}{\sigma} \frac{d\sigma}{dp_L}$ and $\frac{\langle p_T \rangle}{\sigma} \frac{d\sigma}{dp_T}$ versus these variables. The solid curve is the fit obtained in reference 16 using data for production of π^- at energies varying from 13 to 300 GeV. The K_s^o data agrees well with the curve and is an indication of the similarity between the production of π's and K's at high energies. The average values of p_T and p_L for the K_s^o are 0.48 ± 0.04 and 1.01 ± 0.11 GeV/c respectively.

VI. Inclusive Λ^o and $\bar{\Lambda}^o$ Production.

The Λ^o's are produced predominantly in the fragmentation region. The longitudinal rapidity distribution in Fig. 9a shows a peak near y = -2. The exact position of this peak appears to depend upon the associated charge multiplicity n_c. In Fig. 9b $\frac{d\sigma}{dy}$ is plotted separately for Λ^o's with $n_c \leq 6$ and $n_c > 6$. The low multiplicity peak at y = -2.5 is very similar to the one observed in the inclusive production of Δ^{++} [17]. The shift of 1/2 unit in the peak position for the two classes of Λ^o's leads to the speculation that two different production processes may be present. At y less than -2.5 the Λ^o is predominantly associated with events where $n_c \leq 6$. Simple kinematics show that a pion produced in these events has an average rapidity of y = -2, and in the extreme case may have a rapidity that is at most equal to that of the Λ^o. This is consistent with the process where the Λ^o is produced at the target vertex via some fragmentation or exchange mechanism. At the higher multiplicities, where $n_c > 6$, the Λ^o rapidity peaks at y = -2. In this case a pion produced in the same event has on the average, a rapidity that is about the same as the Λ^o. However this pion can have a rapidity that is far more negative than that of the Λ^o. It thus appears that the Λ^o is probably not produced at the target vertex but rather closer to the central region.

In Fig. 9a we also show $\frac{d\sigma}{dy}$ for the $\bar{\Lambda}^o$'s. It is clear that the $\bar{\Lambda}^o$'s are produced entirely in the central region, and the 1 mb cross section is almost exactly equal to that of the Λ^o in the same region. It is worth noting that essentially all the $\bar{\Lambda}^o$'s are produced in events where $n_c \geq 6$. The present data then indicate that all the Λ^o's and $\bar{\Lambda}^o$'s are produced via Λ^o-$\bar{\Lambda}^o$ production in the central region.

The average values of p_T and p_L for the Λ^o are 0.52 ± 0.06 and 4.24 ± 0.62 GeV/c respectively. In Figs. 10a, b, c, and d we show the differential cross sections in terms of x and p_T^2 together with lower energy data. The data appear to have reached scaling limit at Fermilab energies. The data show no correlation between $< n >_{\Lambda^o}$ and $< n_- >$ as shown in Fig. 11 where the straight line fit is consistent with being flat.

We have measured the polarization of the Λ^o. Non-zero inclusive Λ^o polarization has been measured in $\pi^- p$ interactions at 18.5 GeV/c although the $\pi^+ p$ data at this same energy show no polarization[18]. Inclusive Λ^o polarization measurements at higher energies have not been reported. Although our statistics are not large, our data do allow a rough measurement of the Λ^o polarization.

The polarization, P, is measured normal to the plane containing the momenta of the Λ^o and the initial proton. The observed distribution is fitted to a function of the form.

$$\frac{dN}{d\cos\theta_p} = 1 + \alpha P \cos\theta_p$$

where α is assumed to be 0.647[19] and θ_p is the polarization angle defined by

$$\cos\theta_p = \frac{(\vec{p}_i \times \vec{\Lambda}) \cdot \vec{p}_\Lambda}{|\vec{p}_i \times \vec{\Lambda}| \; |\vec{p}_\Lambda|}$$

with $\vec{p}_i$ = incident proton momentum, $\vec{\Lambda}$ = Λ^o momentum in the overall c.m. and $\vec{p}_\Lambda$ = momentum of the proton from Λ^o decay in the Λ^o c.m. The observed distribution is shown in Fig. 12, where the number of Λ^o's corrected for detection efficiency is plotted versus cos θ_p. Corrections for processing loss, normalization, and production in the forward hemisphere are not included. The solid straight line is a best fit yielding $\chi^2 = 1.1$ for $P = 0.34 \pm 0.29$. The dotted line corresponds to zero polarization yielding a $\chi^2 = 2.5$. Thus our results are consistent with zero polarization for the Λ^o. If we restrict our sample to those events for which $|t_{p \to \Lambda^o}| < 2.0$ (GeV/c)^2 we obtain $P = 0.54 \pm 0.43$, again consistent with zero polarization.

Acknowledgements.

We thank the staffs of the accelerator, Neutrino Laboratory, 30-inch Bubble Chamber and Film Analysis Facility at the Fermi National Accelerator Laboratory, for their diligent help during the course of this experiment. We also thank Kwan-Wu Lai and Ricardo Gomez for helpful discussions.

References

1. 102 GeV/c pp: J. W. Chapman et al., Phys. Lett. 47B, 465 (1973).
2. 205 GeV/c pp: G. Charlton et al., Phys. Rev. Lett. 29, 1759 (1972), 30, 574 (1973).
3. 303 GeV/c pp: F. T. Dao et al., Phys. Rev. Lett. 30, 1151 (1973).
4. A. Firestone et al., Phys. Rev. 10D, (in press).
5. The primary vertex fiducial volume was defined as -15 cm $< x <$ 25 cm, -14 cm $< y < -2$ cm, and $0 < z <$ 38 cm. The origin is at the middle of the chamber front glass with the beam going along the negative x direction and z going into the chamber. The V vertex fiducial was defined by $|x^2 + y^2| <$ 28 cm and $0 < z <$ 38 cm.
6. Two constraint classes for each hypothesis were used in the fits. In the 3 constraint fits the mass of the V was assumed to be either that of the γ, K^o, Λ^o or $\bar{\Lambda}^o$. In the 2 constraint fits this mass was left as a free parameter to be determined by the fit.
7. The cuts used on the laboratory transverse momentum between the V and the negative track are $p_T^V < 15$ MeV/c for γ's and $p_T^V > 155$ MeV/c for K_s^o. The kinematic upper limit for the π^- from a Λ^o is $p_T^V = 103$ MeV/c, and about 1% of the Λ^o's have $p_T^V < 15$ MeV/c.
8. The projected distance in the film plane between the V vertex and the primary vertex was required to be greater than 6 cm for γ's with $n_c \leq 6$, 8 cm for $n_c > 6$, 2 cm for K_s^o's, $\bar{\Lambda}^o$'s with $n_c \leq 6$, and 10 cm with $n_c > 6$.
9. T. M. Knasel, DESY Reports 70/2 and 70/3 (1970) unpublished.
10. For a review at various energies see F. T. Dao and J. Whitmore, Phys. Lett. 46B, 252 (1973).
11. D. Cohen, Phys. Lett. 47B, 457 (1973).
12. E. L. Berger, D. Horn and G. H. Thomas, Phys. Rev. 7D, 1412 (1973).

13. F. T. Dao, review talk given at the 1974 meeting of the Division of Particles and Fields of the American Physical Society, Williamsburg, Virginia.

14. F. T. Dao et al., Phys. Lett. 45B, 399 (1973); A. Firestone et al., paper to be submitted to Phys. Rev. Lett. The cross sections used are upper limit estimates after allowing for background subtraction.

15. A. Krzywicki, Nucl. Phys. B58, 633 (1973); E. L. Berger CERN preprint, TH.1737 (1973).

16. F. T. Dao et al., Phys. Rev. Lett. 33, 389 (1974).

17. F. T. Dao et al., Phys. Rev. Lett. 30, 34 (1973).

18. P. H. Stuntebeck et al., Phys. Rev. D9, 608 (1974).

19. Particle Data Group, Phys. Lett. 50B, 1 (1974).

Table 1

Multiplicity Distributions for $pp \rightarrow \gamma$ + n Charged + Anything

n Charged	Number of Observed γ's Used in Analysis (Forward and Backward)	Corrected and Weighted Number	$\langle \gamma \rangle$ / Inelastic n Prong Interaction	σ_n($pp \rightarrow \gamma$ + n Charged + Anything) mb
2	18	2576	4.15 ± 1.12	9.98 ± 2.69
4	45	6330	4.82 ± 0.82	24.51 ± 4.17
6	97	11441	7.58 ± 0.83	44.31 ± 4.87
8	104	12517	8.26 ± 0.91	48.48 ± 5.33
10	87	9998	7.60 ± 0.91	38.72 ± 4.65
12	75	9475	9.97 ± 1.30	36.70 ± 4.77
14	45	6047	9.22 ± 1.66	23.42 ± 4.22
16	26	3198	10.91 ± 2.29	12.39 ± 2.60
18	22	2360	13.80 ± 2.90	9.14 ± 1.92
20	10	967	14.44 ± 4.62	3.75 ± 1.20
22	2	167	3.57 ± 2.57	0.65 ± 0.47
24	2	220	20.03 ± 14.22	0.85 ± 0.61
Total	533	65296	7.84 ± 0.55	257 ± 18

Table 2

Multiplicity Distributions for $pp \rightarrow K^o_s$ + n Charged + Anything

n Charged	Number of Observed K^o_s's Used in Analysis	Corrected and Weighted Number	$< K^o_s >$/ Inelastic n Prong Interaction	$\sigma_n(pp \rightarrow K^o_s$ + n Charged + Anything) mb
2	3	20	0.03 ± 0.02	0.08 ± 0.05
4	19	167	0.13 ± 0.03	0.65 ± 0.15
6	36	316	0.21 ± 0.04	1.22 ± 0.21
8	39	370	0.24 ± 0.04	1.43 ± 0.24
10	40	304	0.23 ± 0.05	1.18 ± 0.27
12	35	320	0.34 ± 0.06	1.24 ± 0.22
14	10	167	0.25 ± 0.09	0.65 ± 0.22
16	2	27	0.09 ± 0.08	0.10 ± 0.08
18	5	70	0.41 ± 0.20	0.27 ± 0.13
20	7	101	1.51 ± 0.61	0.39 ± 0.16
22	0	0	0	0
24	1	12	1.06 ± 1.06	0.05 ± 0.05
Total	197	1874	0.224 ± 0.018	7.34 ± 0.59

Table 3

Multiplicity Distributions for $pp \rightarrow \Lambda^{\circ}$ + n Charged + Anything

n Charged	Number of Observed Λ° Used in Analysis	Corrected and Weighted Number	$< \Lambda^{\circ} > /$ Inelastic n Prong Interaction	$\sigma_n (pp \rightarrow \Lambda^{\circ}$ + n Charged + Anything) mb
2	5	43	0.06 ± 0.03	0.17 ± 0.08
4	15	133	0.10 ± 0.03	0.51 ± 0.14
6	17	154	0.10 ± 0.03	0.60 ± 0.15
8	15	137	0.09 ± 0.03	0.53 ± 0.15
10	16	168	0.13 ± 0.03	0.65 ± 0.17
12	13	116	0.13 ± 0.04	0.45 ± 0.13
14	6	90	0.14 ± 0.06	0.35 ± 0.16
16	1	12	0.04 ± 0.04	0.05 ± 0.05
18	2	31	0.18 ± 0.14	0.12 ± 0.09
20	1	23	0.34 ± 0.34	0.09 ± 0.09
Total	91	907	0.11 ± 0.01	3.61 ± 0.35

Figure Captions

Fig. 1 Longitudinal rapidity distribution for inclusive γ's.

Fig. 2 $\frac{< n >}{< n_I >} \frac{\sigma_I(n)}{\sigma_{inel}}$ versus $\frac{n}{< n >}$ for π^o, K_s^o and Λ^o. $< n >$ and $< n_I >$ are the average numbers per inelastic collision for charged particles and the inclusive particle considered, $\sigma_I(n)$ is the inclusive cross section associated with n charged particles and σ_{inel} is the total inelastic cross section. The curve is a fit from reference 10 using inclusive π^o data from pp and $\bar{p}p$ experiments.

Fig. 3
a. The average number of π^o's produced per inelastic interaction plotted as a function of negative charge multiplicity. The straight line is a linear fit to the data.

b. The average number of π^o's produced per non-diffractive inelastic interaction versus the negative charge multiplicity. The straight line is the best fit to a constant $< n_o >$. The open circles indicate upper limits for $< n_o >_{non}$.

Fig. 4. Inclusive distributions for $pp \rightarrow \gamma$ + anything.

a. $\frac{1}{\sigma_{inel}} \frac{d\sigma}{dx}$ versus x. b. $\frac{1}{\sigma_{inel}} \frac{d\sigma}{dp_T^2}$ versus p_T^2.

c. The invariant cross section integrated over p_T^2 versus x.

d. The invariant cross section integrated over x versus p_T^2.

Fig. 5 Longitudinal rapidity distribution for inclusive K_s^o's.

Fig. 6 The average number of K_s^o's produced per inelastic interaction plotted as a function of negative charge multiplicity. The straight line is a linear fit to the data.

Fig. 7 Inclusive distributions for $pp \to K_s^o$ + anything.

a. $\frac{1}{\sigma_{inel}} \frac{d\sigma}{dx}$ versus x. b. $\frac{d\sigma}{dp_T^2}$ versus p_T^2.

c. The invariant cross section integrated over p_T^2 versus x.

d. The invariant cross section integrated over x versus p_T^2.

Fig. 8 a. $\frac{< p_L >}{\sigma} \frac{d\sigma}{dp_L}$ versus $\frac{p_L}{< p_L >}$. b. $\frac{< p_T >}{\sigma} \frac{d\sigma}{dp_T}$ versus $\frac{p_T}{< p_T >}$.

for the reaction $pp \to K_s^o X$. The solid curves are fits from reference 15.

Fig. 9 a. Longitudinal rapidity distributions for Λ^o and $\bar{\Lambda}^o$.

b. Same distributions for the Λ^o plotted separately for charge multiplicity $n_c \leq 6$ and $n_c > 6$. The dotted and solid lines are drawn to guide the eye.

Fig. 10 Inclusive distributions for $pp \to \Lambda^o$ + anything.

a. $\frac{1}{\sigma_{inel}} \frac{d\sigma}{dx}$ versus x. b. $\frac{d\sigma}{dp_T^2}$ versus p_T^2.

c. The invariant cross section integrated over p_T^2 versus x.

d. The invariant cross section integrated over x versus p_T^2.

Fig. 11 The average number of Λ^o's produced per inelastic interaction plotted as a function of negative charge multiplicity. The straight line is a linear fit to the data.

Fig. 12 Polarization angular distribution of the Λ^o. The polarization angle θ_p is defined in the text. The solid line is the best linear fit to the data with polarization parameter $P = 0.34 \pm 0.29$. The dotted line corresponds to $P = 0$.

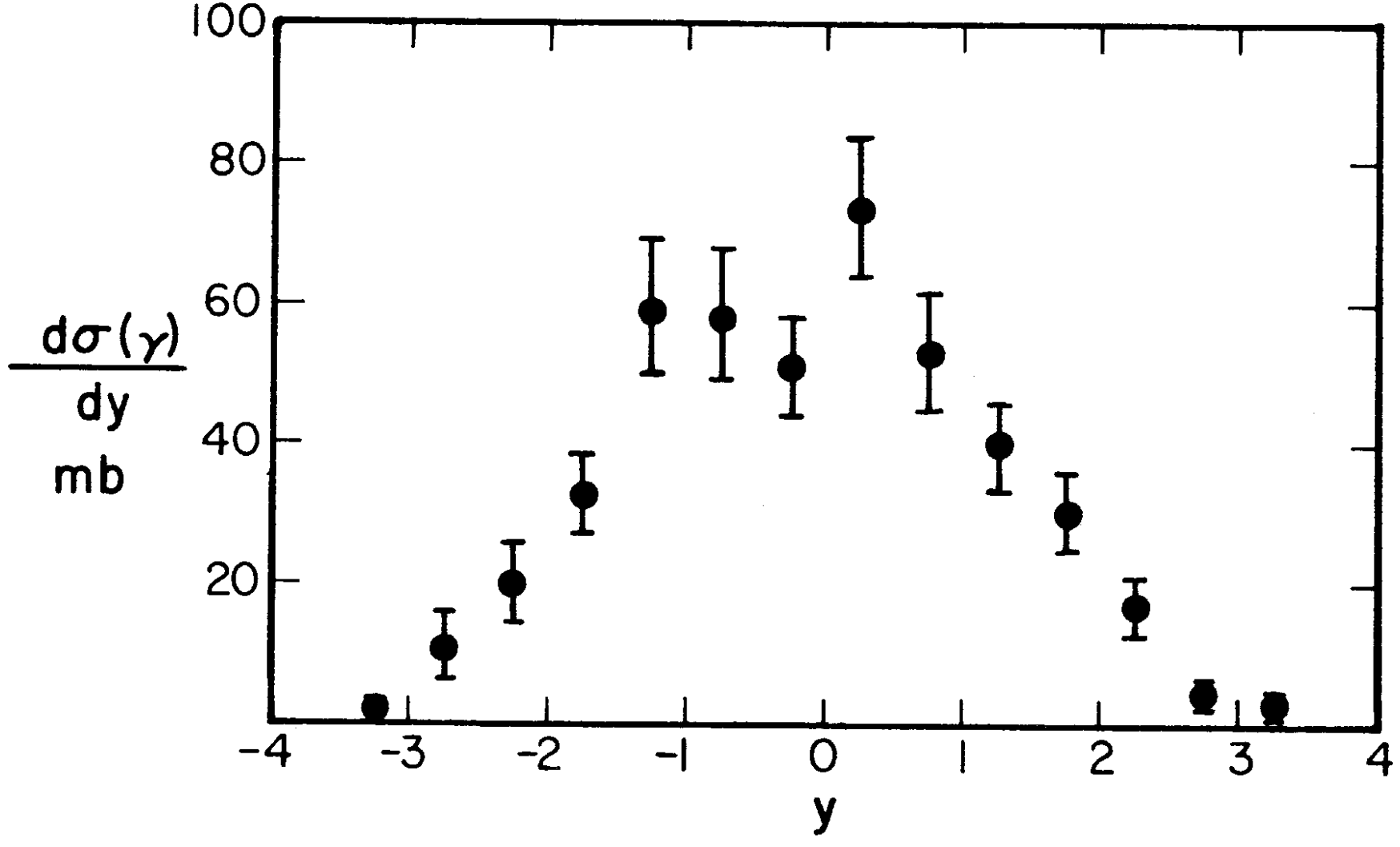

Fig. 1

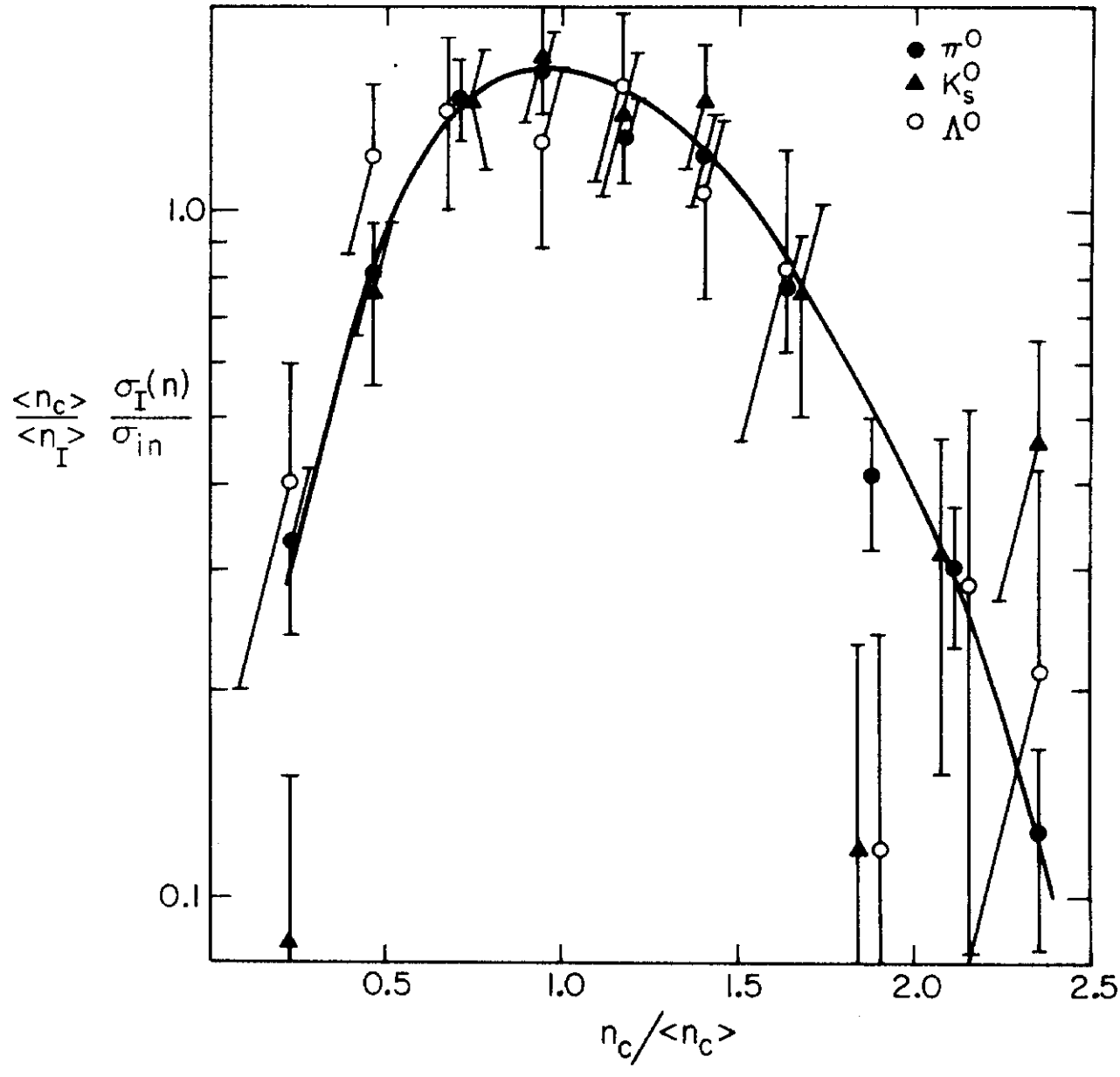
π^0
K_s^0
Λ^0
1.0
0.1
$\frac{<n_c>}{<n_I>}\ \frac{\sigma_I(n)}{\sigma_{in}}$
0.5
1.0
1.5
2.0
2.5
$n_c/<n_c>$

Fig. 2

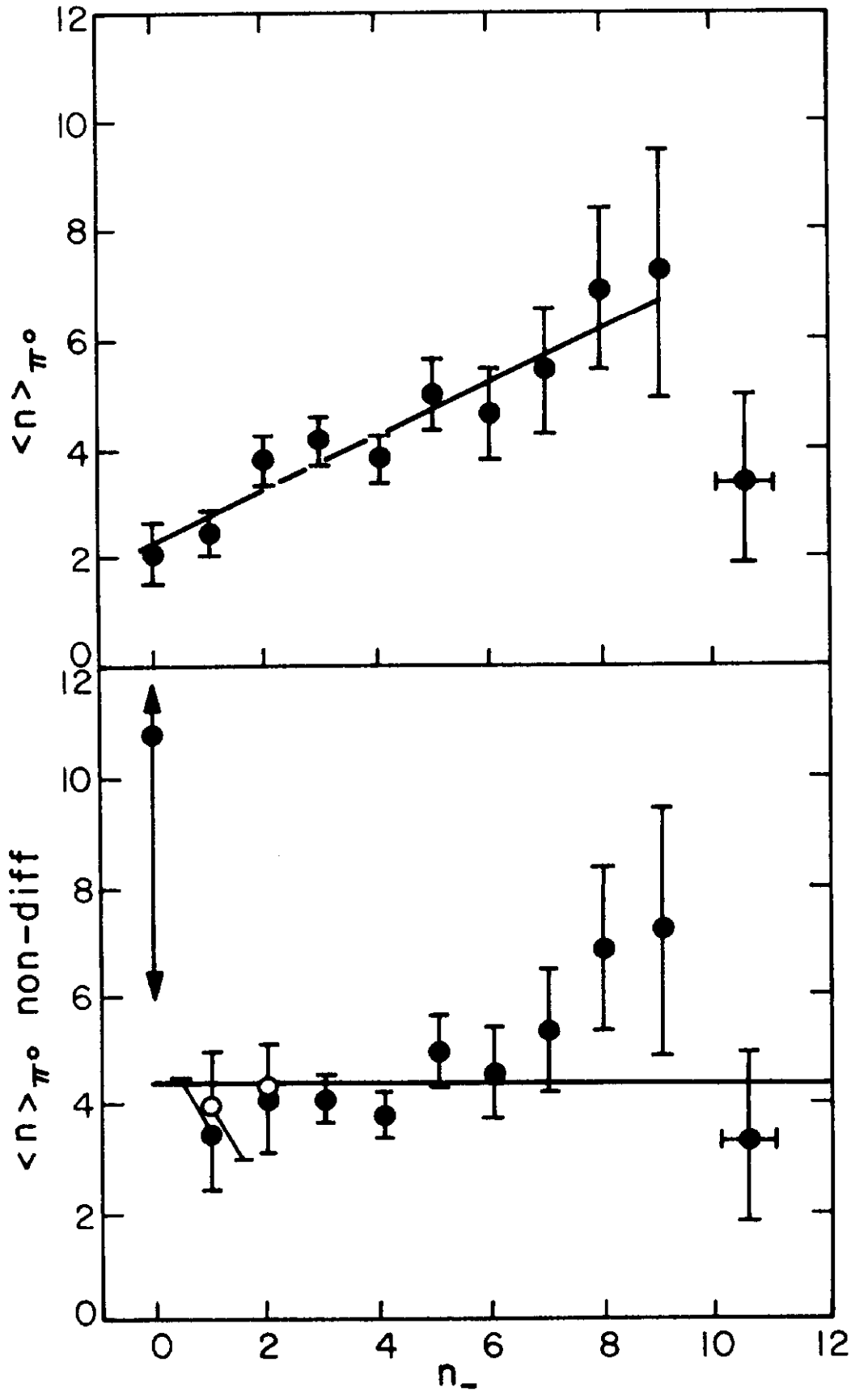
12
10
8
6
4
2
0
$\langle n \rangle_{\pi^0}$
12
10
8
6
4
2
0
$\langle n \rangle_{\pi^0}$ non-diff
0
2
4
6
8
10
12
n_-

Fig. 3

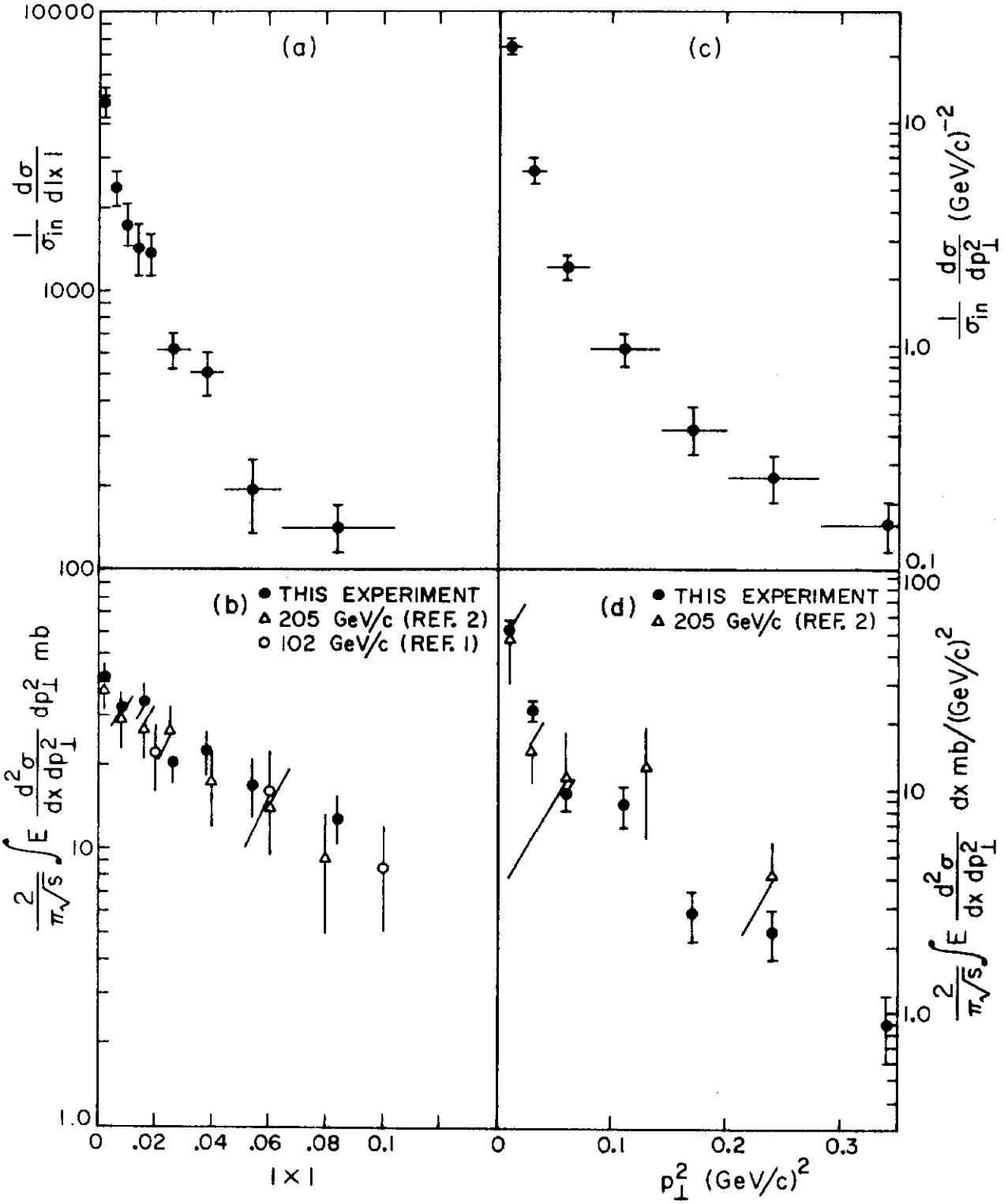
(a)
(c)
(b)
(d)
THIS EXPERIMENT
205 GeV/c (REF. 2)
102 GeV/c (REF. 1)
$\frac{1}{\sigma_{in}}\frac{d\sigma}{d|x|}$
$\frac{1}{\sigma_{in}}\frac{d\sigma}{dp_\perp^2}$ (GeV/c)$^{-2}$
$\frac{2}{\pi\sqrt{s}}\int E\frac{d^2\sigma}{dx\,dp_\perp^2}dp_\perp^2$ mb
$\frac{2}{\pi\sqrt{s}}\int E\frac{d^2\sigma}{dx\,dp_\perp^2}dx$ mb/(GeV/c)^2
$|x|$
$p_\perp^2$ (GeV/c)^2

Fig. 4

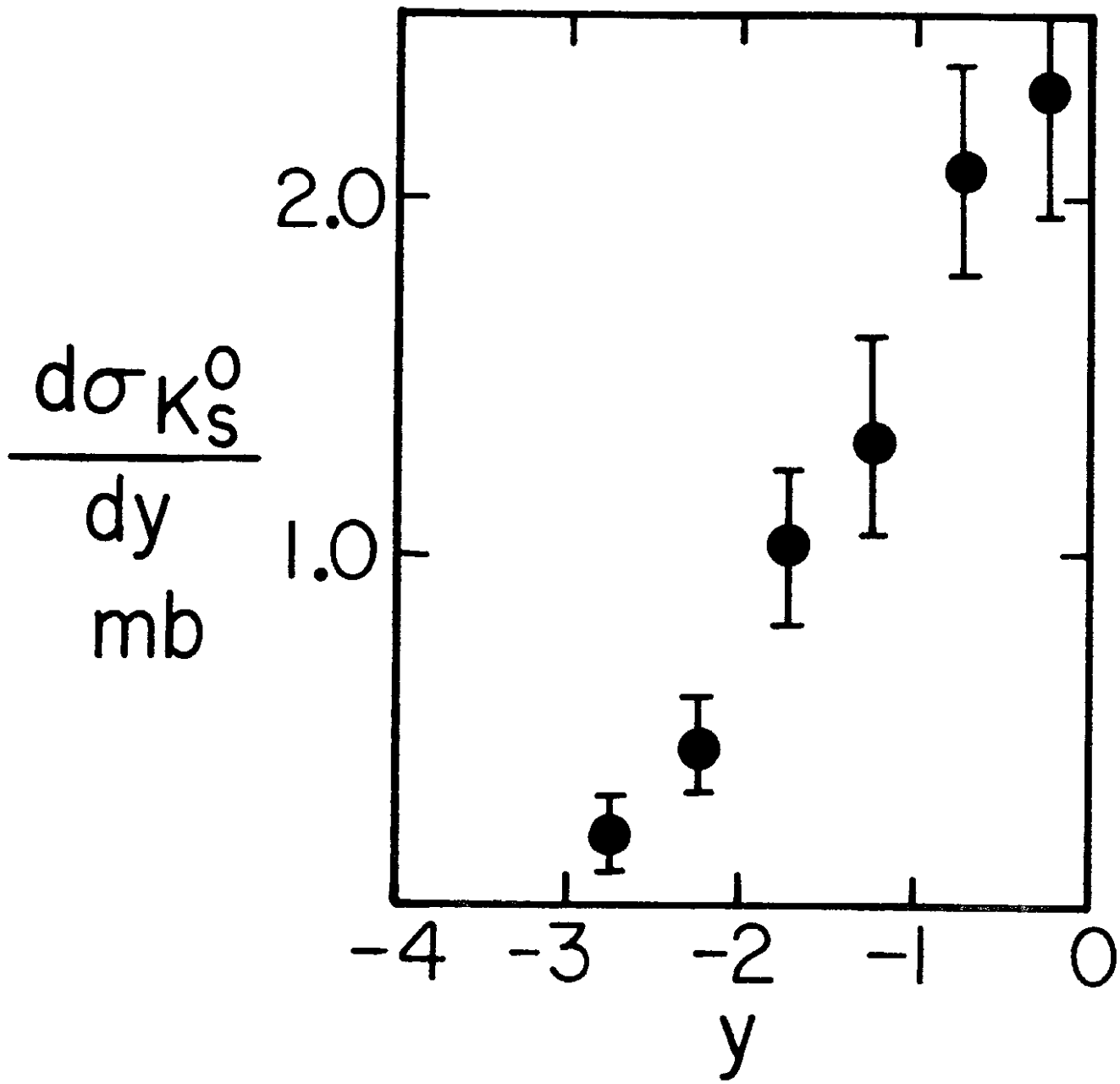

Fig. 5

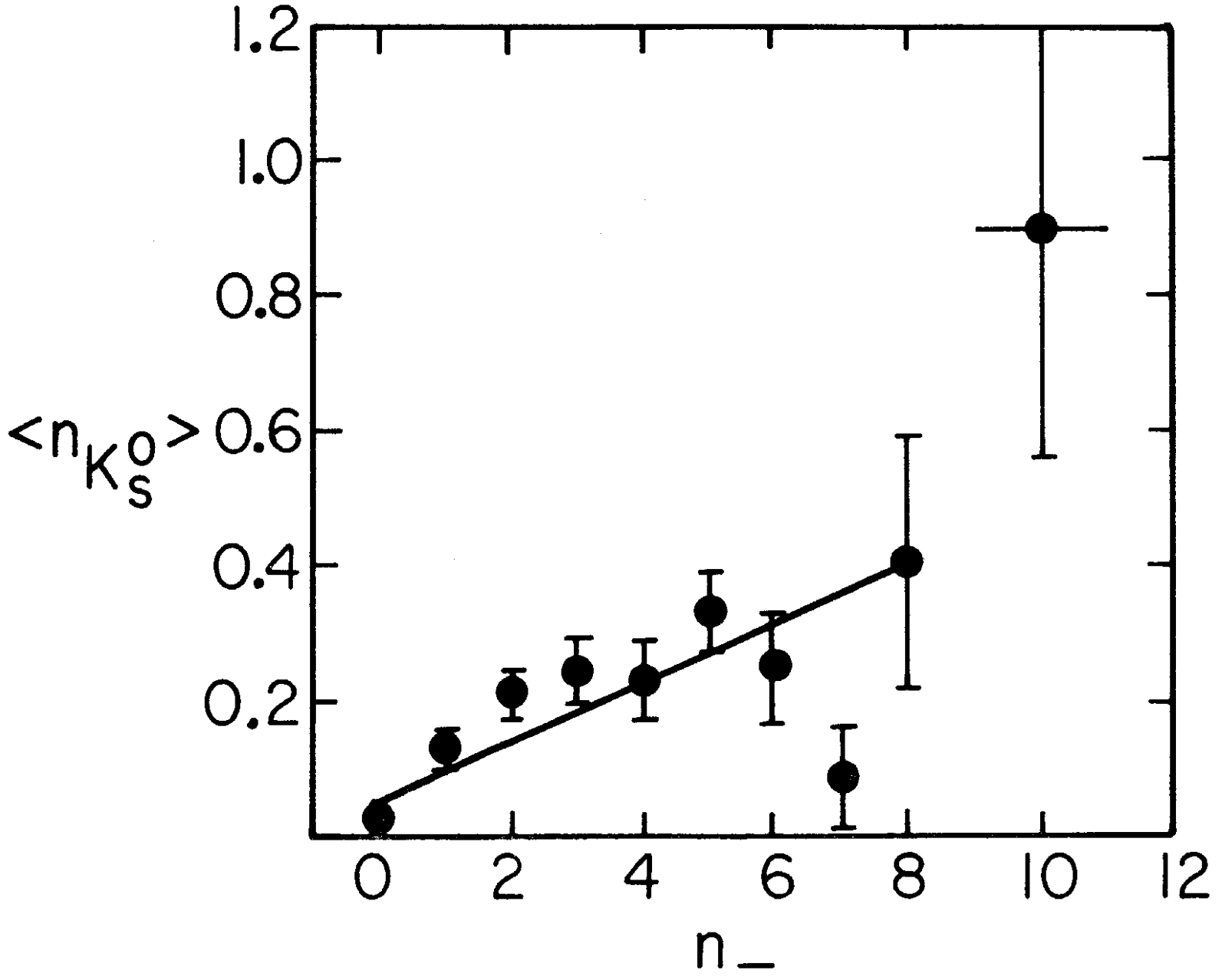

Fig. 6

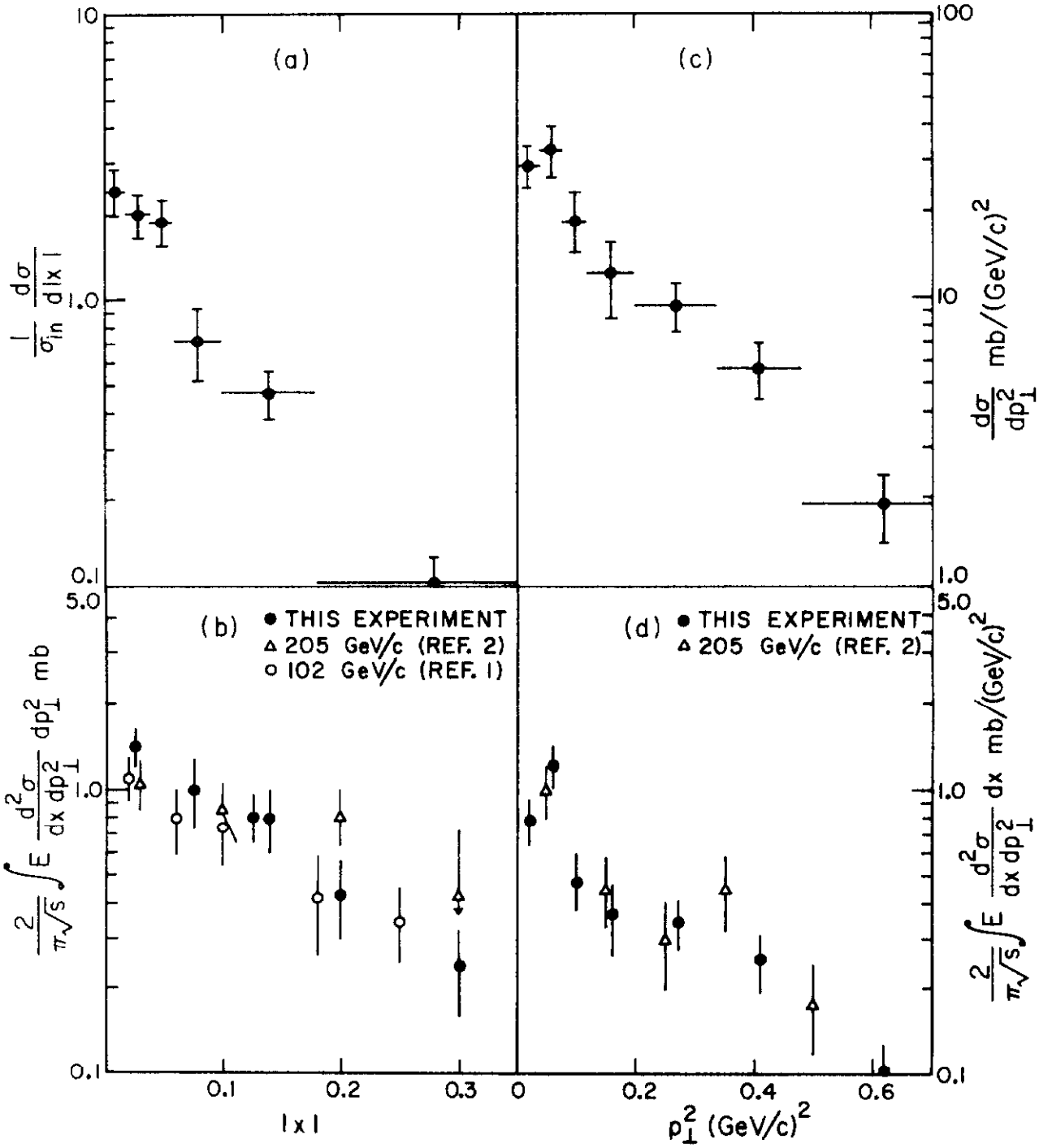
(a)
(b)
(c)
(d)
● THIS EXPERIMENT
△ 205 GeV/c (REF. 2)
○ 102 GeV/c (REF. 1)
● THIS EXPERIMENT
△ 205 GeV/c (REF. 2)
$\frac{1}{\sigma_{in}}\frac{d\sigma}{d|x|}$
$\frac{d\sigma}{dp_\perp^2}$ mb/(GeV/c)^2
$\frac{2}{\pi\sqrt{s}}\int E\frac{d^2\sigma}{dx\,dp_\perp^2}dp_\perp^2$ mb
$\frac{2}{\pi\sqrt{s}}\int E\frac{d^2\sigma}{dx\,dp_\perp^2}dx$ mb/(GeV/c)^2
|x|
$p_\perp^2$ (GeV/c)^2

Fig. 7

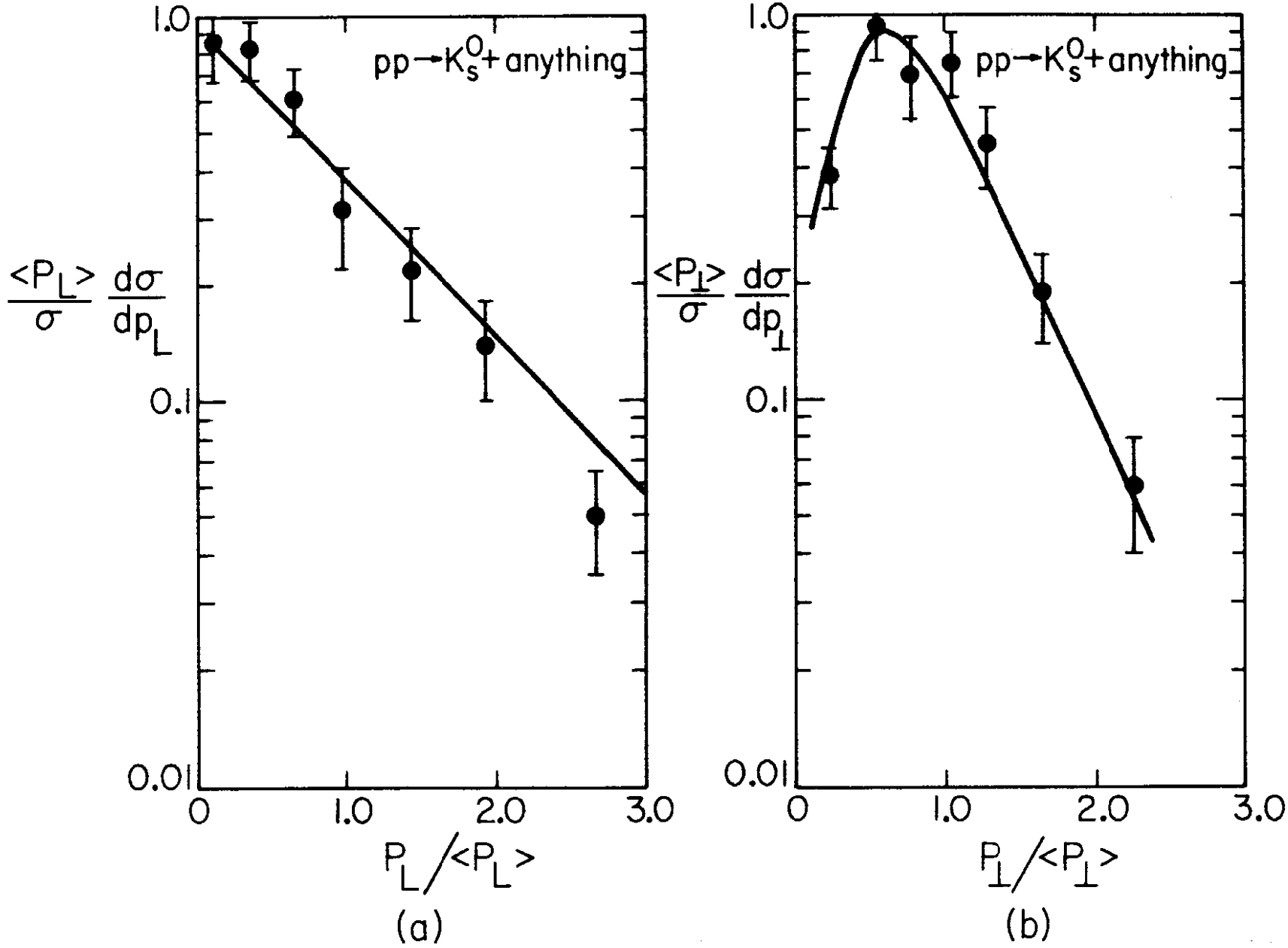
1.0
0.1
0.01
pp→K^0_s+anything
$\frac{\langle P_L \rangle}{\sigma} \frac{d\sigma}{dp_L}$
0
1.0
2.0
3.0
$P_L/\langle P_L \rangle$
(a)
$\frac{\langle P_\perp \rangle}{\sigma} \frac{d\sigma}{dp_\perp}$
$P_\perp/\langle P_\perp \rangle$
(b)

Fig. 8

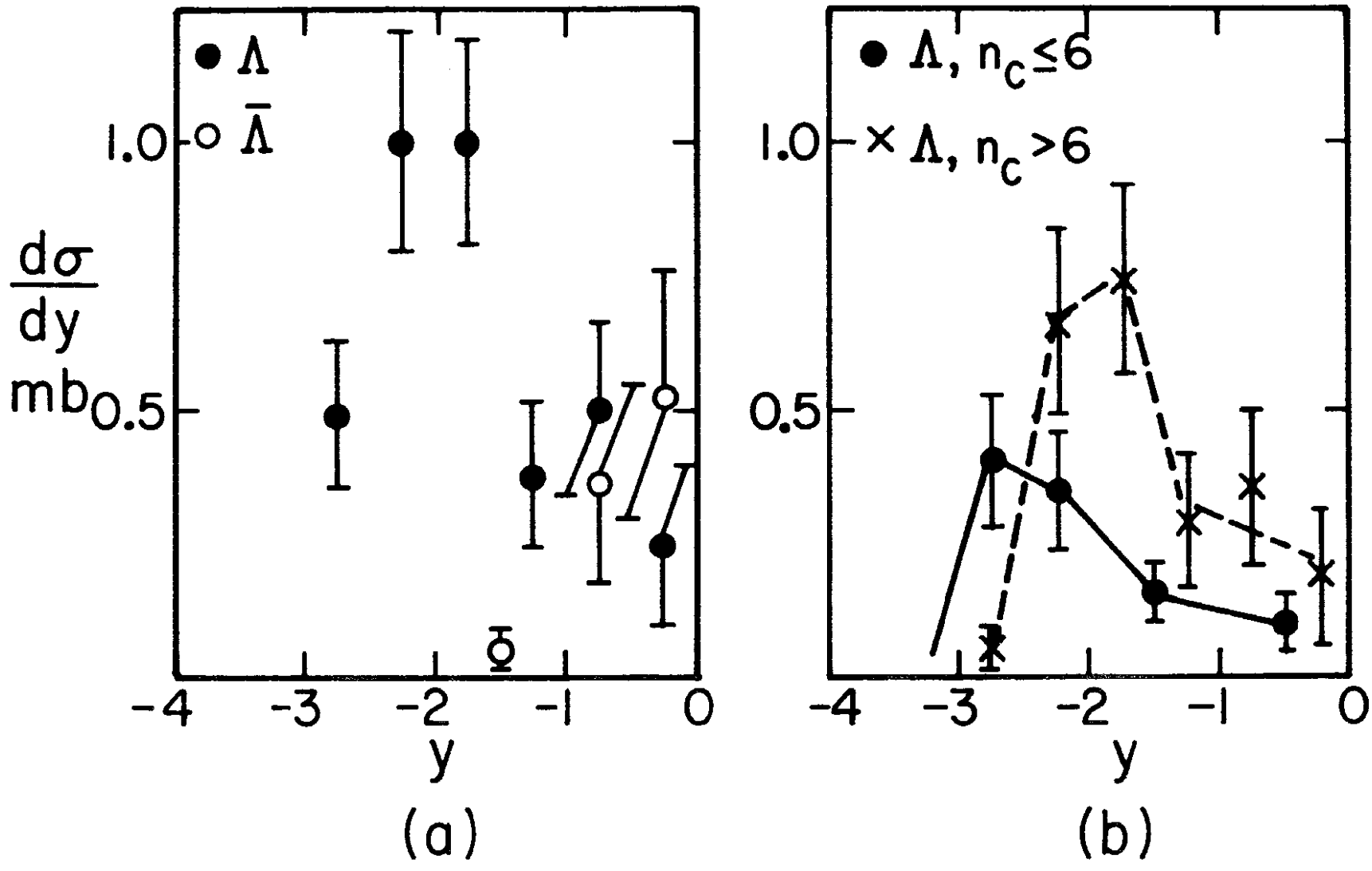
● Λ
○ $\bar{\Lambda}$
1.0
0.5
$\frac{d\sigma}{dy}$ mb
-4
-3
-2
-1
0
y
(a)
● Λ, $n_c \leq 6$
× Λ, $n_c > 6$
1.0
0.5
-4
-3
-2
-1
0
y
(b)

Fig. 9

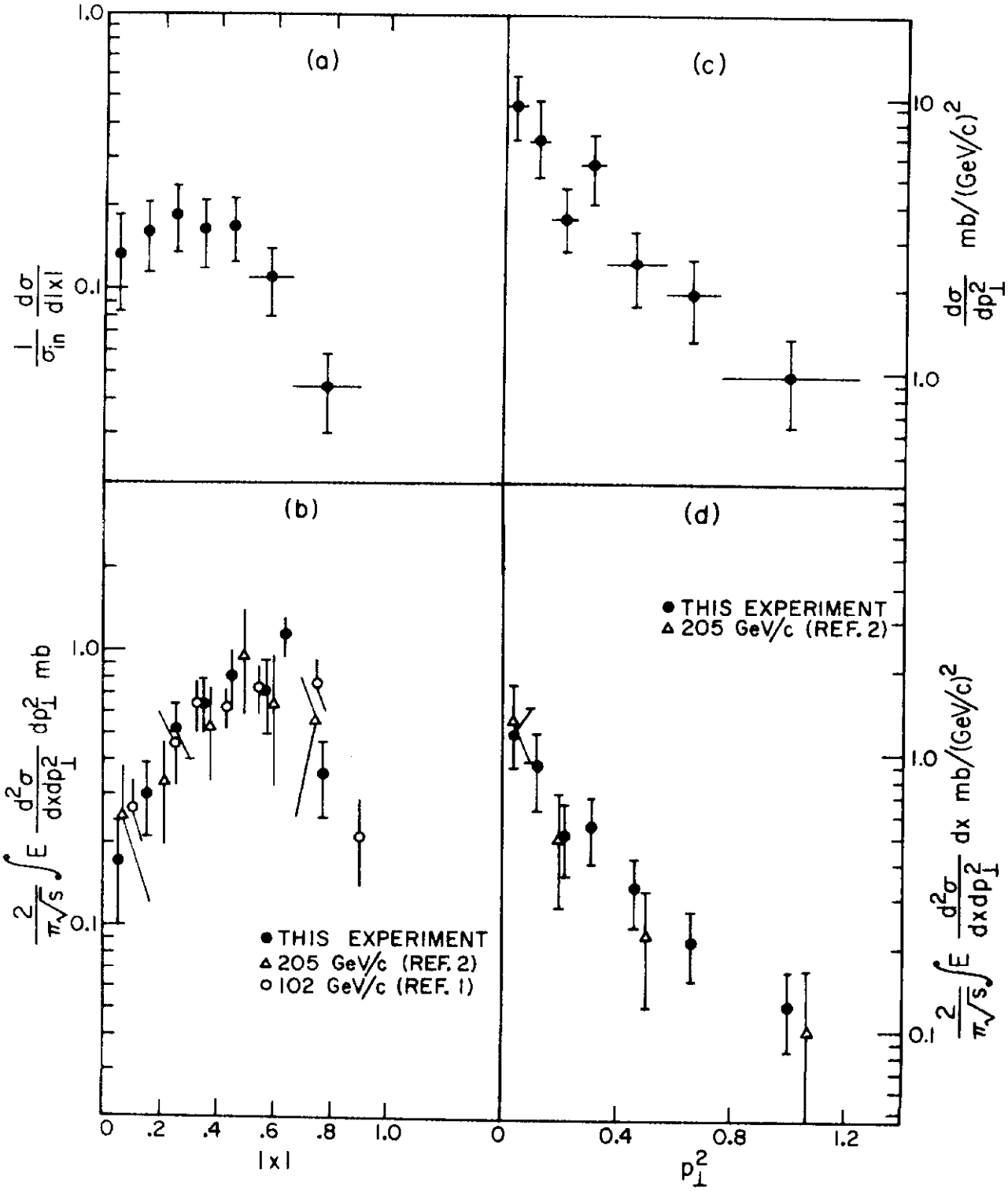
(a)
(b)
(c)
(d)
$\frac{1}{\sigma_{in}}\frac{d\sigma}{d|x|}$
$\frac{2}{\pi\sqrt{s}}\int E\frac{d^2\sigma}{dx dp_\perp^2}dp_\perp^2$ mb
$\frac{d\sigma}{dp_\perp^2}$ mb/(GeV/c)^2
$\frac{2}{\pi\sqrt{s}}\int E\frac{d^2\sigma}{dx dp_\perp^2}dx$ mb/(GeV/c)^2
|x|
$p_\perp^2$
● THIS EXPERIMENT
△ 205 GeV/c (REF. 2)
○ 102 GeV/c (REF. 1)
● THIS EXPERIMENT
△ 205 GeV/c (REF. 2)

Fig. 10

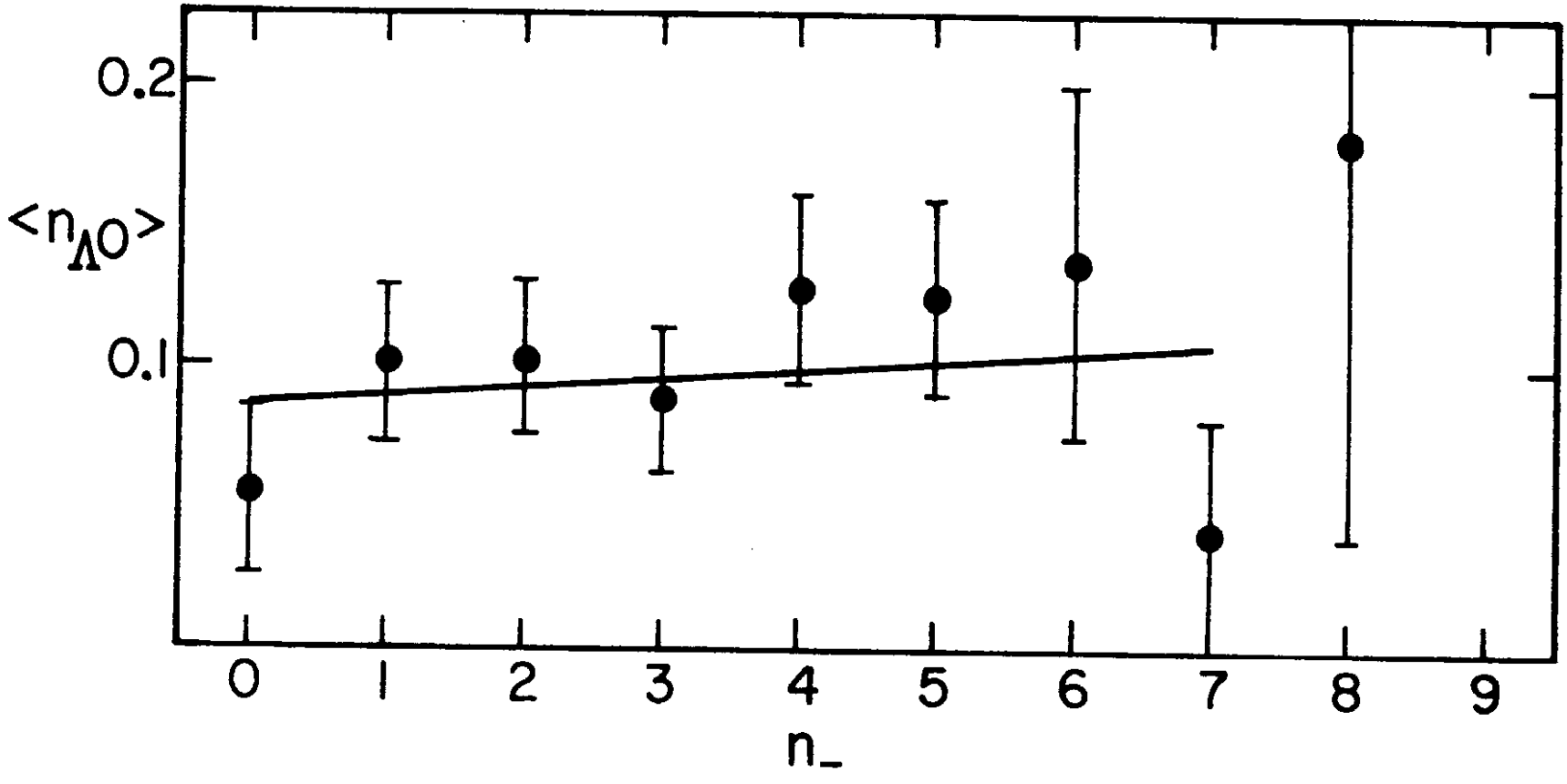

Fig. 11

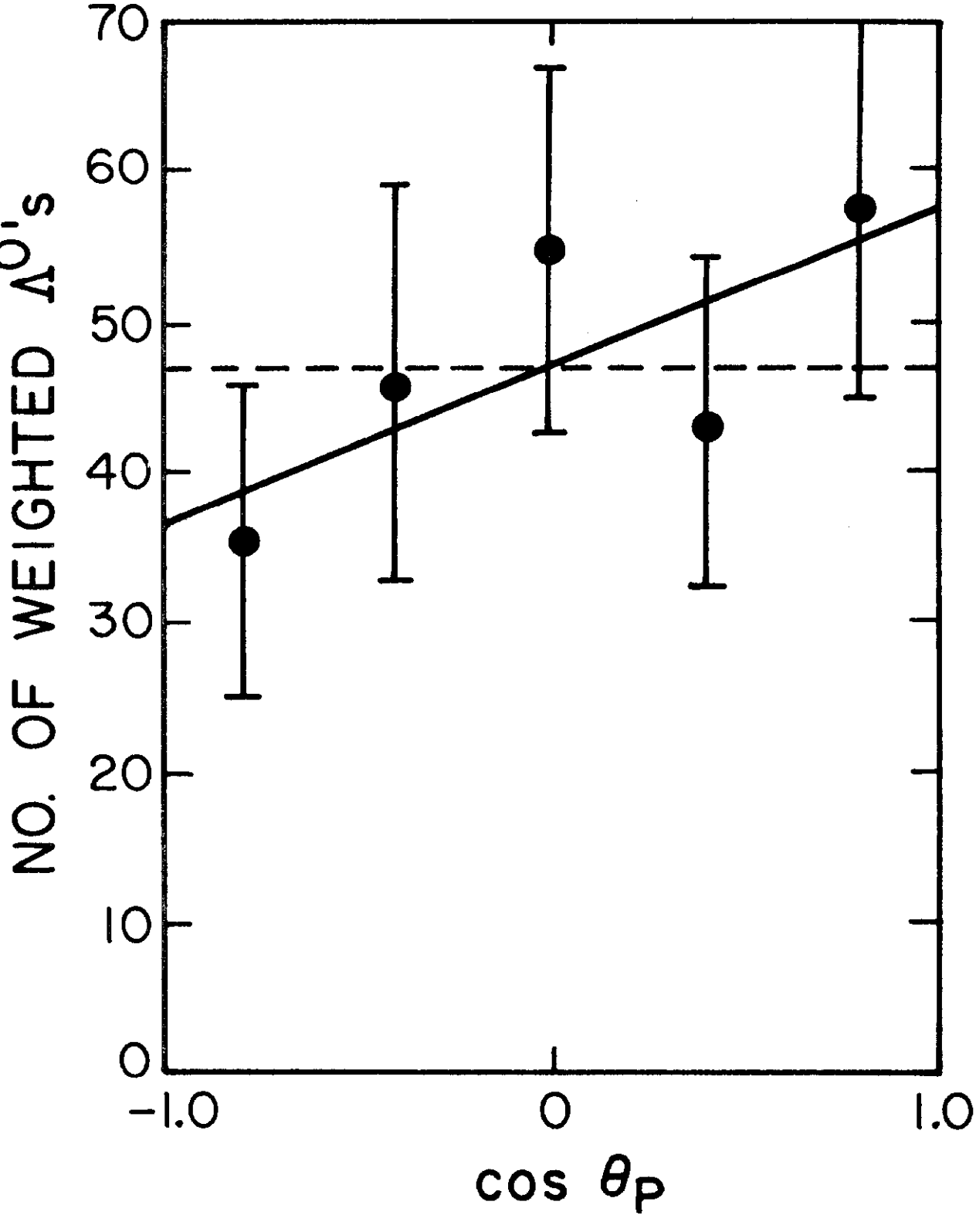

Fig. 12